14th International Symposium on Turbulence and Shear Flow Phenomena (TSFP14)
Heidelberg, Germany, July 28–31, 2026

NEW OBSERVATIONS ON STRAIN RATE DYNAMICS NEAR INHOMOGENEOUS FLUID INTERFACES

Pedro D. Alves
IDMEC
Instituto Superior Técnico, Universidade de Lisboa
Lisboa, Portugal
pedrodalves@tecnico.ulisboa.pt

Oliver R. H. Buxton
Department of Aeronautics
Imperial College London
London SW7 2AZ, UK
o.buxton@imperial.ac.uk

Carlos B. da Silva
IDMEC
Instituto Superior Técnico, Universidade de Lisboa
Lisboa, Portugal
carlos.silva@tecnico.ulisboa.pt

ABSTRACT

Direct numerical simulations (DNSs) of a spatially-developing turbulent/turbulent interface (TTI) and a temporally-developing turbulent/non-turbulent interface (TNTI) are used to study the dynamics of the rate-of-strain tensor, s_{ij}, in the vicinity of these inhomogeneous regions. It is shown that the conditional profiles of the strain rate magnitude, s^2, in a TNTI resemble those of a TTI once its outermost surface is considered to be located further into the turbulent bulk flow. Moreover, the conditional profiles of the eigenvalues of s_{ij} in a TTI have similarities with those of a TNTI, however shifted towards the rotational background. By projecting the s_{ij} governing equation onto its eigenframe, we confirm that the peak of self-amplification in s^2 is mostly due to a compressive motion. By contrast, the vorticity stretching mechanism benefits from all three eigenvalues, with the intermediate one playing a paramount role near the strain-dominated region. Finally, a simple *toy model* based on the coexistence of two different vortices in a two-layer turbulent background is shown to provide a qualitatively good agreement with the DNS results.

INTRODUCTION

Turbulent/turbulent interfaces (TTIs) exist when turbulent regions with different turbulence characteristics interact. These appear in a multitude of canonical flows, ranging from turbulent wakes to boundary layers under free-stream turbulence. TTIs are a generalisation of the denominated turbulent/non-turbulent interfaces (TNTIs), which occur between a turbulent region and an irrotational background (da Silva *et al.*, 2014*a*). Although studies on the dynamics of TNTIs have been developed since the 1950s, after the seminal work of Corrsin & Kistler (1955), research devoted to the dynamics of TTIs is recent, with most efforts having started in the 2020s, after the experimental study of Kankanwadi & Buxton (2020).

So far, research on TTIs has unveiled some of the key differences and similarities between these interfaces and TNTIs. Namely, it has been observed that the viscous diffusion of the small-scale quantities of enstrophy, $\omega_i\omega_i$, and strain rate magnitude, $s_{ij}s_{ij}$, where $\omega_i \equiv \varepsilon_{ijk}\partial u_k/\partial x_j$ is the vorticity field, $s_{ij} \equiv (\partial u_i/\partial x_j + \partial u_j/\partial x_i)/2$ is the rate-of-strain tensor, and u_i is the velocity field, are negligible across TTIs (Kankanwadi & Buxton, 2022; Alves *et al.*, 2025). This is in contrast with what occurs in a TNTI (Holzner *et al.*, 2009), where viscous phenomena dominate the outermost part of the interface. Besides, TTIs showcase an enhanced $s_{ij}s_{ij}$ in the interfacial region (Kankanwadi & Buxton, 2022; Alves *et al.*, 2025), which distinguishes these from TNTIs. In spite of that, when the conditional profiles of $\omega_i\omega_i$ and the interface-normal distance are normalised, respectively, by the local Kolmogorov time and length scales, $\tau_\eta = (\nu/\varepsilon)^{1/2}$, and $\eta = (\nu^3/\varepsilon)^{1/4}$, where ν is the kinematic viscosity and $\varepsilon = 2\nu\langle s_{ij}s_{ij}\rangle$ is the viscous dissipation rate of turbulent kinetic energy (with $\langle\cdot\rangle$ being a suitable average), universal profiles (although different for each case) are retrieved for both TNTIs (Zecchetto & da Silva, 2021) and TTIs (Nakamura *et al.*, 2023; Chen & Buxton, 2024; Alves *et al.*, 2025). Despite much being known about the characterisation of TTIs, a deeper understanding of the flow physics behind some of these observations is lacking. In particular, the reason for the increased strain rate in the vicinity of a TTI remains unclear. Moreover, a conceptual bridge that could explain the universality and link the two types of interfaces is required.

To this end, this work focuses in providing a new perspective on the dynamics of the rate-of-strain tensor, which is the source of the greatest dissimilarities between TNTIs and TTIs. Thus, we first start by assessing the impact of conditioning the rate-of-strain magnitude jump in TNTIs to increasing levels of vorticity thresholds, and compare the profiles with those typically observed in a TTI. Then, we decompose s_{ij} into its eigenvalues, σ_i, to study their evolution across both TNTIs and TTIs. Motivated by the complex nature of straining motions near TTIs, we then further dive into the dynamics of σ_i by explicitly assessing the terms of their governing equations, and compare these with their counterparts for the total rate-of-strain magnitude, as first proposed in Alves *et al.* (2026). Consequently, we provide a mechanistic model of TTIs that showcases the most relevant small-scale flow features, based

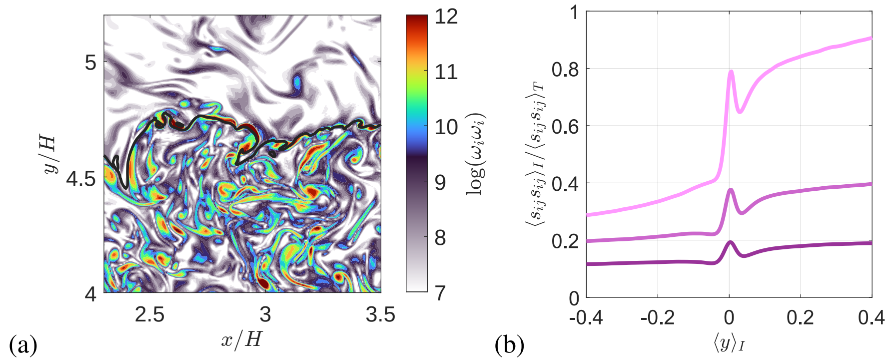

Figure 1. (a) Two-dimensional cut of the (logarithm of) enstrophy. The RB is highlighted by the black solid line. The colorbar limits were adjusted to depict regions with $\log(\omega_i\omega_i) \leq 7$ as white. (b) Conditional profiles of rate-of-strain tensor magnitude for three streamwise stations normalised by the inner layer turbulent core region of the first station.

on the observations previously drawn. Finally, we point out the main conclusions and propose some directions for future work.

DIRECT NUMERICAL SIMULATIONS

To carry out this study, we analyse two direct numerical simulations (DNSs). The first is a spatially-decaying TTI with $2048 \times 1024 \times 1024$ grid points, and a maximum inlet Taylor-based Reynolds number of $Re_\lambda \sim 194$. To generate the initial condition we run: *(i)* two precursor temporally-developing statistically stationary DNSs of homogeneous isotropic turbulence (HIT) with different properties, namely longitudinal integral length scale, L_{11}, velocity root-mean-square (rms), u', and vorticity rms, ω'. Then, at each time instant, we impose in the inlet of a *(ii)* spatially-developing DNS a plane of velocity fluctuations composed of one of the precursor simulations in the interval $-\pi/2 \leq y \leq \pi/2$ (inner layer), and elsewhere of the other simulation (outer layer). Further details and validations can be found in Alves *et al.* (2025). Notice that the TTI herein analysed corresponds to the case denoted by $T^{l\omega u}_{l\Omega U}$ in that work.

The second DNS is a temporally-developing TNTI with $1024 \times 1024 \times 1024$ grid points and $Re_\lambda \sim 260$ (at the instant of analysis). The initial condition is similar to the shear-free turbulence case reported in Zecchetto & da Silva (2021). Essentially, the initial velocity field is given by the convolution of a temporally-developing DNS of HIT with a profile that maintains the velocity fluctuations in the interval $-\pi/4 \leq y \leq \pi/4$ and sets it to zero in the remaining volume of the domain. The parameters, for both DNSs, are shown in table 1.

Table 1. Parameters of each simulation: the longitudinal integral length scale, L_{11}, the root-mean-square (rms) vorticity, ω', and rms velocity, u'. The superscripts (O) or (I) refer to the parameters of the outer or inner layer siding the TTIs, respectively.

Simulation	$L_{11}^{(\mathrm{O})}/L_{11}^{(\mathrm{I})}$	$\omega'^{(\mathrm{O})}/\omega'^{(\mathrm{I})}$	$u'^{(\mathrm{O})}/u'^{(\mathrm{I})}$
TTI	0.47/0.46	67.1/149.4	1.8/3.2
Simulation	L_{11}	ω'	u'
TNTI	1.20	83.7	3.0

To identify the rotational boundary (RB) of the TTI, i.e. the surface that separates the two turbulent regions, we resort to an isosurface of passive scalar ϕ with unity Schmidt number. In particular, we consider a threshold value of $\phi_{\mathrm{th}} = 0.5$, for a normalised field $\phi \in [0;1]$, to distinguish the RB. Analogously, to identify the irrotational boundary (IB) of the TNTI, i.e. the outermost surface that separates the turbulent bulk flow from the irrotational background, an isosurface of vorticity magnitude is used, following the procedure developed in Taveira *et al.* (2013). These boundaries are important as they allow for the statistics of the relevant variables to be conditioned to the interface-normal distance. For the remainder of the manuscript, any quantity taken in this manner will be denoted as $\langle\cdot\rangle_I$.

In figure 1a, a two-dimensional cut close to the inlet of the spatially-developing DNS is shown. The different levels of enstrophy in the outer/inner layers are clear, and so is the separation granted by the passive scalar isosurface. In turn, the conditional profiles of $s_{ij}s_{ij}$ (figure 1b) show a non-monotonous trend, with a noticeable enhanced strain rate magnitude close to the RB, i.e. $\langle y\rangle_I = 0.0$, for all streamwise distances.

CONNECTION BETWEEN TNTIS AND TTIS

Firstly, we shall focus in trying to understand the connection between TNTIs and TTIs as seen from the strain rate magnitude. Indeed, this quantity is the source of the greatest differences: whereas TNTIs exhibit a rather smooth monotonically-increasing evolution of $s_{ij}s_{ij}$ (Zecchetto & da Silva, 2021), TTIs show the aforementioned enhanced peak of strain rate magnitude close to the RB (figure 1b). To explain this behaviour, let us start by recalling that we often rely on the volume fraction function, $\mathrm{Vol}(|\omega|^*)$, where $|\omega|^*$ is the vorticity magnitude independent variable, to define the IB of a TNTI (da Silva *et al.*, 2014*b*). This function quantifies the normalised fraction of the total domain volume that has $|\omega| \geq |\omega|^*$. For example, if $|\omega_*| = 0.0$, then $\mathrm{Vol}(|\omega|^*) = 1.0$ while if $|\omega_*| = \max(|\omega|)$, then $\mathrm{Vol}(|\omega|^*) = 0.0$. The threshold used to identify the IB, $|\omega|_{\mathrm{th}}$, shall then belong to a *plateau* region, i.e. a range of vorticity magnitudes for which the volume fraction is fairly insensitive to the specific value of $|\omega|^*$, which attests to the idea of the TNTI being a region characterising a sharp transition between two adjacent fluid streams. If we choose increasingly higher values of $|\omega|_{\mathrm{th}}$, outside this range, we are considering an IB further inside the bulk turbulent flow. In other words, the *irrotational* background in the vicinity of the TNTI exhibits a non-negligible vorticity magnitude in this case.

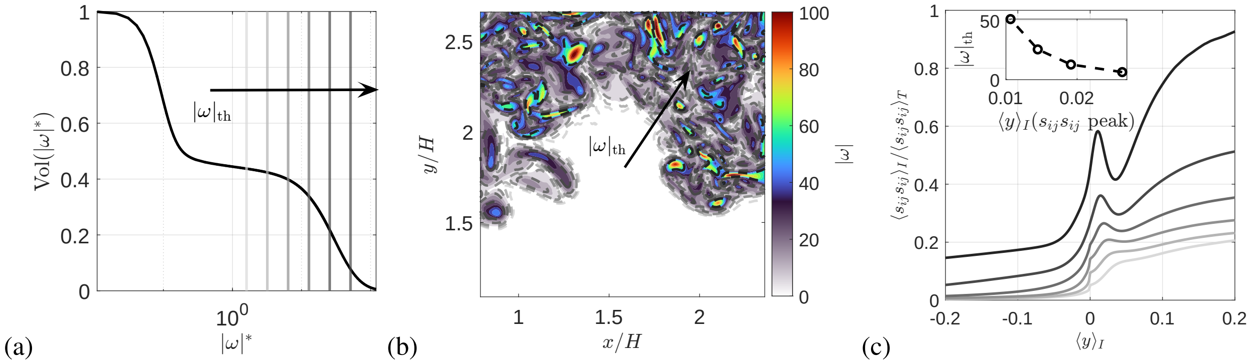

Figure 2. Effect of the vorticity magnitude threshold (a) on the volume fraction function, (b) in a two-dimensional cut of vorticity magnitude, and (c) on the conditional profiles of rate-of-strain tensor magnitude. Lighter to darked shades of gray correspond to increasing levels of thresholds in the range $|\omega|_{\rm th} \in \{1.6; 3.2; 6.4; 12.8; 25.6; 51.2\}$. The inset highlights position of the local s^2 maximum.

We applied this idea to the temporally-developing DNS which exhibits a TNTI, and chose six different thresholds $|\omega|_{\rm th} \in \{1.6; 3.2; 6.4; 12.8; 25.6; 51.2\}$ (figure 2a). The first two belong to the *plateau* region and correspond to approximately 0.43 of the total volume, whereas the other four correspond to Vol$(|\omega|^*) \in [0.07; 0.40]$. This has a clear and visual impact on the IB (figure 2b). As $|\omega|_{\rm th}$ increases, the IB approaches the coherent vortical structures of the flow until it eventually surrounds only the most intense ones. It happens that this also yields a dramatic effect on the conditional profiles of $s_{ij}s_{ij}$. Most noticeably, we observe the emergence a local maximum of $s_{ij}s_{ij}$ with an adjacent local minimum, and a non-null value of $s_{ij}s_{ij}$ for $\langle y\rangle_I < 0$ (figure 2c). For the first two thresholds these features are yet absent (as the thresholds belong to the *plateau* region). From $|\omega|_{\rm th} = 6.4$ onwards, a peak appears in the high-$|\omega|$ side, and the strain rate tensor magnitude does not decay to zero in the low-$|\omega|$ region, mirroring qualitatively the typical profiles of a TTI (figure 1b). In the inset of figure 2c we show the threshold used for identifying the IB as a function of the location of the $s_{ij}s_{ij}$ peak. It is clear that it is moving towards the IB ($\langle y\rangle_I = 0$) with increasing $|\omega|_{\rm th}$. This analysis extends the postulate made in Alves *et al.* (2025), concerning the interpretation of a TTI as being a TNTI where the difference in the enstrophy levels on both sides of the interface were taken *ad extremum*. Here, the argument is used in the reverse order, i.e. if we allow for the difference in the enstrophy levels in a TNTI to diminish, we recover the typical profile of a TTI. This has some interesting consequences on the definition of interfacial thicknesses (when measured using local scales, and not those defined with values of the turbulent core region). Indeed, a local increased $\langle s_{ij}s_{ij}\rangle_I$ will yield a smaller local Kolmogorov scale, since $\langle\eta\rangle_I \equiv (\nu^2/\langle 2s_{ij}s_{ij}\rangle_I))$. Therefore, the universal collapse of enstrophy by the Kolmogorov time scale, $\langle\omega_i\omega_i\rangle_I\langle\tau_\eta\rangle_I^2$, which is expressed in terms of the non-dimensional interface-normal coordinates $\langle y\rangle_I/\langle\eta\rangle_I$ will be *compressed*. Notice that this observation does not affect the universal shape of the conditional enstrophy profiles normalised using local Kolmogorov scales.

In light of the connection between TNTIs and TTIs, it is reasonable to ask whether one of the s_{ij} eigendirections is more responsible for this phenomenon than another. Thus, we now compare the typical dynamics of the rate-of-strain tensor eigenvalues. Henceforth, in terms of notation, we assume $\sigma_1 \geq \sigma_2 \geq \sigma_3$, with $\sigma_1 > 0$ the most extensive and $\sigma_3 < 0$ the most compressive strain rate tensor eigenvalues. In figure 3a, conditional profiles of σ_i normalised by their value at the turbulent core are shown for the TTI and the TNTI of Elsinga & da Silva (2019). For a turbulent/non-turbulent interface, the evolution of the most extensive eigenvalue from the turbulent core to the IB is characterised by a slow decrease up to $13\langle\eta\rangle_I$, followed by an increase up to $6\langle\eta\rangle_I$. Then, it rapidly decays towards the irrotational background. The intermediate eigenvalue has a similar trend, although more feeble extremi, and a slower decay as $\langle y\rangle_I \to -\infty$. In comparison, for a turbulent/turbulent interface, we observe qualitatively similar features, with stronger peaks and valleys of both σ_1 and σ_2, although in different locations. Indeed, whereas for a TNTI the dynamics are mostly encapsulated in the rotational region, in the case of a TTI, these are shifted towards the outer layer. We can offer the following interpretation of this occurrence: the mechanisms of a TNTI are mostly uni-directional, from irrotationality to turbulence. When rotationality starts appearing in the background, it draws the dynamics to this region, shortening a layer that is reminiscent of a TNTI. This adds to the picture in Chen & Buxton (2024), where two layers are proposed based on the normalisation of enstrophy by the rate-of-strain magnitude.

DYNAMICS OF THE RATE-OF-STRAIN TENSOR EIGENVALUES NEAR TTIS

Although arguments were made that the TTI-like behaviour can be retrieved from turbulent/non-turbulent interfaces if more permissive vorticity magnitude thresholds are chosen, the fact is that the enhanced $s_{ij}s_{ij}$ is seen in at the RB of a TTI and not at the IB of a TNTI. This carries some implications on the higher-order terms governing the rate-of-strain tensor magnitude, e.g. its production via self-amplification, $P_s \equiv -2s_{ij}s_{jk}s_{ki}$, will exhibit a pronounced growth (Alves *et al.*, 2025). Thus, we need a method that gives us more insight into the physics of s_{ij} that a simple scalar analysis of its magnitude does not give. To this end, we can further detail the role of each σ_i by taking the rate-of-strain governing equation, and projecting it onto its eigenframe, following Nomura & Post (1998); Carbone *et al.* (2020). If we then take the inner product with σ_i, a budget equation for σ_i^2 appears (Alves

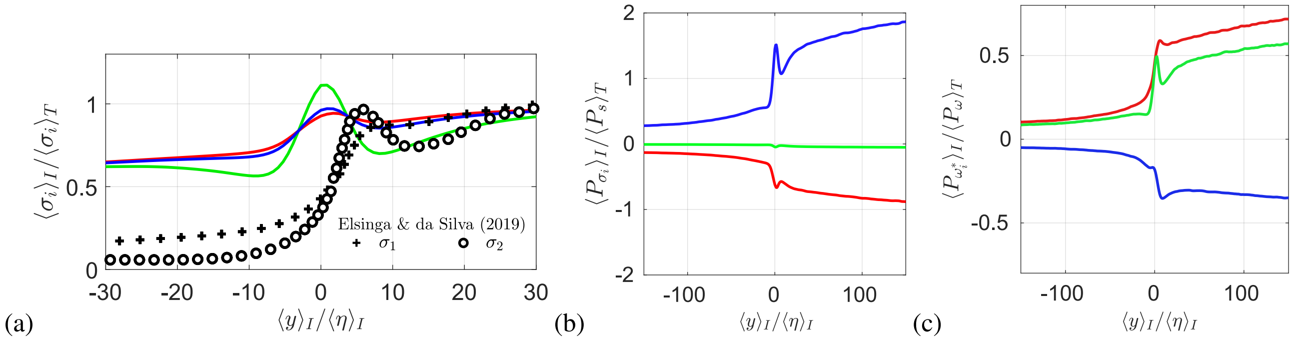

Figure 3. Conditional profiles of (a) rate-of-strain tensor eigenvalues normalised by their turbulent core value for three streamwise distances for TTIB34. The profiles for a TNTI reported in Elsinga & da Silva (2019) are also shown. Conditional profiles of (a) strain rate eigenvalue self-amplification and (b) enstrophy production per strain rate eigenvalue normalised the corresponding terms for the total strain rate magnitude taken at the turbulent core. The colours red/green/blue correspond to the most extensive/intermediate/most compressive directions.

et al., 2026),

$$\begin{aligned}\underbrace{\frac{D}{Dt}\left(\sigma_i^2\right)}_{T_{\sigma_i}} = & \underbrace{-2\sigma_i^3}_{P_{\sigma_i}} \underbrace{+\frac{1}{2}\sigma_i\omega_k^*\omega_k^*}_{P^{(\mathrm{proj})}_{\omega_i^*}/2} \underbrace{-\frac{1}{2}\sigma_i\omega_{(i)}^*\omega_{(i)}^*}_{-P_{\omega_i^*}/2} \\ & \underbrace{-2\sigma_{(i)}H_{i(i)}^*}_{D_{\sigma_i}^{(p)}} \underbrace{+\nu\frac{\partial^2}{\partial x_k\partial x_k}\left(\sigma_i^2\right)}_{D_{\sigma_i}^{(\nu)}} \underbrace{-2\nu\frac{\partial\sigma_i}{\partial x_k}\frac{\partial\sigma_{(i)}}{\partial x_k}}_{E_{\sigma_i}},\end{aligned} \qquad (1)$$

where the superscript $*$ denotes a quantity written in the basis formed by the rate-of-strain eigenvalues, e_{ij}, i.e. $\omega_i^* = \mathrm{e}_{ji}\omega_j$ and $H_{ij}^* = \mathrm{e}_{ki}H_{kl}\mathrm{e}_{lj}$. Notice that the index written inside parenthesis is not contracted. Here, T_{σ_i} represents the total temporal variation of the eigenvalue magnitude $\sigma_i\sigma_{(i)}$, P_{σ_i} represents its production due to self-amplification, $P^{(\mathrm{proj})}_{\omega_i^*}$ relates to a projection of each eigenvalue on the total enstrophy (written in the eigenvalue's basis), $P_{\omega_i^*}$ is the production of enstrophy, i.e. vorticity stretching, $D_{\sigma_i}^{(p)}$ accounts for the diffusion of each eigenvalue due to the interaction with pressure, $D_{\sigma_i}^{(\nu)}$ is the viscous diffusion of eigenvalue magnitude and E_{σ_i} the viscous dissipation. By virtue of the consistency in the projection, if we sum the terms of a given mechanism for the three eigenvalues, we obtain the corresponding evolution for the total rate-of-strain tensor magnitude, e.g. $P_s = P_{\sigma_1} + P_{\sigma_2} + P_{\sigma_3}$. As such, in figure 3b, we show the ratio of local eigenvalue to turbulent core strain rate magnitude self-amplifications, i.e. $\langle P_{\sigma_i}\rangle_I/\langle P_s\rangle_T$. It is clear that the peak of rate-of-strain self-amplification observed at the RB (cf. figure 19b of Alves *et al.* (2025)) is due to σ_3, while the most extensive direction, σ_1, depleting it the most intensely. Interestingly, due to incompressibility, i.e. $\sigma_1+\sigma_2+\sigma_3 = 0$), the term $P^{(\mathrm{proj})}_{\omega_i^*}$ sums up to zero for the three components, as it is equal to $(\sigma_1+\sigma_2+\sigma_3)\omega_k^*\omega_k^*$. Thence, in figure 3c, we present conditional profiles of the local ratio of enstrophy production per eigenvalue to the turbulent core total one, $\langle P_{\omega_i^*}\rangle_I/\langle P_\omega\rangle_T$. Here, the intermediate eigenvalue has a major contribution, especially at the RB. Close to the peak of rotationality, i.e. $\langle y\rangle_I \approx 7\langle\eta\rangle_I$ its significance is greatly reduced, exhibiting a valley, while that of P_{σ_3} increases (in absolute value).

MECHANISTIC MODEL OF TTIS

To capture the strikingly rich strain-rate dynamics that were unveiled in the previous sections, we propose a simple analytical model. Essentially, it amounts to considering the joint superposition of two vortical structures within a two-layer turbulent background. The former assumes two different Burgers (1948) vortices. These are placed in a three-dimensional space (x,y,z), one with an axis aligned with the z-direction located at $(x_\mathrm{O},0,0)$, where $x_\mathrm{O} < 0$, and another parallel to the previous at $(x_\mathrm{I},0,0)$, where $x_\mathrm{I} > 0$. Each one has a different circulation, Γ_O or Γ_I, radius, R_O or R_I, or stretching rate, α_O or α_I, respectively. The new velocity field is assumed to be composed of the sum of those imprinted by each vortex. In the end, we can derive an analytical expression for the total enstrophy and rate-of-strain magnitude, detailed in Alves *et al.* (2026). In figure 4a, we show the evolution of ω^2 for a set of co-rotating vortical structures, i.e. $\Gamma_\mathrm{I}\Gamma_\mathrm{O} > 0$, with variables based on those used in the DNS (table 1). When there exists the greatest dissimilarity in the levels of ω_O^2 and ω_I^2 (light curves), the qualitative shape agrees remarkably well with the DNS curves presented in Alves *et al.* (2025). As for the rate-of-strain magnitude (figure 4b), we capture a small peak at $x \approx 0$, which adds on to the interpretation previously put forward concerning the emergence of a local $s_{ij}s_{ij}$ peak.

CONCLUSION

The results presented herein on the rate-of-strain dynamics add to the decades of research devoted to the study of inhomogeneous sharp fluid interfaces. Indeed, the relation between TNTIs and TTIs shown via the effect of vorticity magnitude threshold as well as the evolution of the rate-of-strain tensor eigenvalues, points out the underlying similarities and differences between these layers. This sets an unprecedented baseline which allows the interpretation of sharp interfaces as a unique field within the broader area of inhomogeneous turbulence. Moreover, the detailed analysis of TTIs, as seen from the rate-of-strain tensor eigenvalues, provides answers that a mere scalar observation of the total magnitude cannot offer. Namely, we understand the compressive nature of the enhanced rate-of-strain tensor magnitude near a TTI and the importance of three orthogonal directions for producing enstrophy. On top of that, it proves to be a valuable tool to use in other settings that benefit from a preferential orientation of the eigenvalues with respect to a local direction. Lastly, the analytical model, in spite of its simplicity, captured the small-

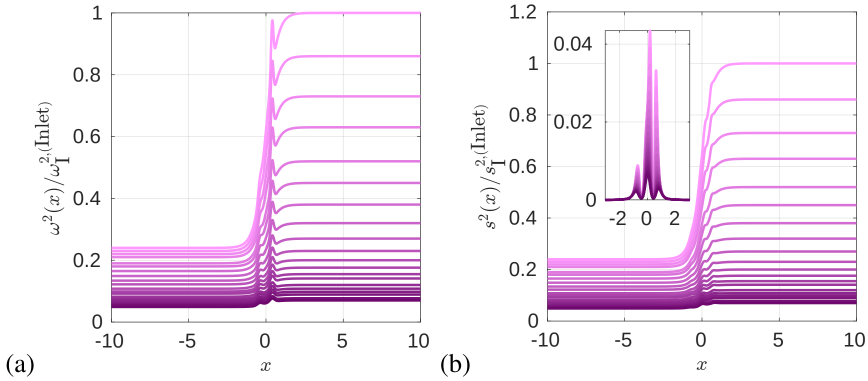

Figure 4. Conditional profiles of (a) enstrophy and (b) rate-of-strain magnitude provided by the analytical model, for a set of parameters similar to those reported in figure 14e of Alves *et al.* (2025). The inset shows the rate-of-strain profiles due to the vortical-induced behaviour only.

scale dynamics of TTIs, and opens the door to the study of structure-based models of turbulence, with more details described in Alves *et al.* (2026).

ACKNOWLEDGMENTS

Pedro D. Alves acknowledges Maria Neves for providing the data of the shear-free turbulence DNS.

REFERENCES

Alves, P. D., Buxton, O. R. H. & da Silva, C. B. 2026 Inhomogeneity and anisotropy of the straining motions near turbulent interfaces. *(Under review in J. Fluid Mech.)* .

Alves, P. D., Zecchetto, M., Buxton, O. & da Silva, C. B. 2025 Dynamics of spatially developing turbulent/turbulent interfaces in the absence of mean shear. *J. Fluid Mech.* **1022**, A9.

Burgers, J. M. 1948 A mathematical model illustrating the theory of turbulence. *Advances in applied mechanics* **1**, 171–199.

Carbone, M., Iovieno, M. & Bragg, A. D. 2020 Symmetry transformation and dimensionality reduction of the anisotropic pressure hessian. *J. Fluid Mech.* **900**, A38.

Chen, J. & Buxton, O. R. H. 2024 Turbulent/turbulent entrainment in a planar wake. *J. Fluid Mech.* **1000**, A26.

Corrsin, S. & Kistler, A. L. 1955 Free-stream boundaries of turbulent flows. *Tech. Rep.*.

Elsinga, G. E. & da Silva, C. B. 2019 How the turbulent/non-turbulent interface is different from internal turbulence. *Journal of Fluid Mechanics* **866**, 216–238.

Holzner, M., Lüthi, B., Tsinober, A. & Kinzelbach, W. 2009 Acceleration, pressure and related quantities in the proximity of the turbulent/non-turbulent interface. *J. Fluid Mech.* **639**, 153–165.

Kankanwadi, K.S. & Buxton, O.R.H. 2020 Turbulent entrainment into a cylinder wake from a turbulent background. *J. Fluid Mech.* **905**, A35.

Kankanwadi, K.S. & Buxton, O.R.H. 2022 On the physical nature of the turbulent/turbulent interface. *J. Fluid Mech.* **942**, A31.

Nakamura, K., Watanabe, T. & Nagata, K. 2023 Turbulent/turbulent interfacial layers of a shearless turbulence mixing layer in temporally evolving grid turbulence. *Phys. Fluids* **35** (4).

Nomura, K. K. & Post, G. K. 1998 The structure and dynamics of vorticity and rate of strain in incompressible homogeneous turbulence. *J. Fluid Mech.* **377**, 65–97.

da Silva, C.B., Hunt, J.C.R., Eames, I. & Westerweel, J. 2014*a* Interfacial layers between regions of different turbulence intensity. *Annu. Rev. Fluid Mech.* **46**, 567–590.

da Silva, C. B., Taveira, R. R. & Borrell, G. 2014*b* Characteristics of the turbulent/nonturbulent interface in boundary layers, jets and shear-free turbulence. In *Journal of Physics: Conference Series*, , vol. 506, p. 012015. IOP Publishing.

Taveira, R. R., Diogo, J. S., Lopes, D. C. & da Silva, C. B. 2013 Lagrangian statistics across the turbulent-nonturbulent interface in a turbulent plane jet. *Phys. Review E* **88** (4), 043001.

Zecchetto, M. & da Silva, C. B. 2021 Universality of small-scale motions within the turbulent/non-turbulent interface layer. *J. Fluid Mech.* **916**, A9.